Journal of Engineering Research and Education
Volume 16, 2024 [76-87]

Effects of Air Vortex Finder Length and Outlet Diameter Variations on Oil Palm Loose Fruit Collector

Adam Danial Lim bin Jefri Lim[1,2], and Saiful Anuar bin Abu Bakar[1*]

[1] Department of Aeronautics, Automotive and Ocean Engineering,
Faculty of Mechanical Engineering, Universiti Teknologi Malaysia,
81310, Skudai, Johor, Malaysia.

[2] Department of Agricultural and Biosystems Engineering,
Faculty of Engineering, Universiti Putra Malaysia,
43400, UPM Serdang, Selangor, Malaysia.

ABSTRACT

Oil palm is one of the largest economy sectors in Malaysia. Among the problems faced in the estates are oil palm loose fruits deposition which is currently being collected manually in the industry. Hence, an oil palm loose fruit collector is designed using cyclone separator mechanism and was studied using computational fluid dynamics (CFD). In the current study, Reynold's stress model (RSM) and the Discrete phase model (DPM) was employed to navigate numerical simulations where the vortex finder of the cyclone separator was varied with two factors which are the vortex finder length and outlet diameter. Wall was set to a no slip condition with standard wall functions. Hydraulic diameter of the gas outlet is B_c=0.1 m. Hydraulic diameters of the particle's outlet are J_c=0.15 m and 0.2 m respectively. Turbulence intensity at the gas and particles outlet are specified at 5%. An injection with density 995.7 kg/m^3 and 0.04 m was set to simulate oil palm loose fruit collection into the system. Ultimately, effects of vortex finder and outlet variations on the pressure drop and collection efficiency were then analyzed. Results indicate that an outlet diameter of 0.18 m and vortex finder length of 0.405 m is favourable for the oil palm loose fruit machine with a collection efficiency of 88.71 % and pressure drop of 477.66 Pa.

Keywords: Computational fluid dynamics, cyclone separator, discrete phase model, oil palm loose fruits, reynold's stress model

1. INTRODUCTION

Oil palm is one of the main agricultural crops planted in Malaysia, covering 5,865,297 hectares of land in the nation. From the total planted area, 72.2% is of plantations comprised by private and government estates, 16.6% belonged to independent small holders while the remaining 11.5 % belongs to organized small holders [1]. In general, the oil palm industry is categorized into upstream and downstream divisions. The upstream comprises of activities conducted in plantations and transportations to the palm mills whereas downstream activities begin in the mill. According to Yusoff *et al*., [2], the activities involved upstream in plantations are cutting fresh fruit bunches, frond stacking, fresh fruit bunches collection, loose fruit collection and lastly transportations of harvests to the mill.

Generally, the reason to collect oil palm loose fruits is to avoid losses as the fruits produces high oil extraction rate (OER) due to its ripeness [3-4]. Sime Darby [5], stated that OER per weight ratio of loose fruits stands at 40 %, while Shuib *et al*., [6], stated that the outer layer of bunches gives out almost 50 % of the total oil percentage in a bunch Therefore, if loose fruits are not collected, the total OER of fruit bunches will drop as the portion that make up the highest OER are not included.

*Corresponding author: saifulanuar@utm.my

This is further supported by Chang *et al*., [7], that reported loose fruit collection as one of the factors directly affecting OER. The current method of collection is manually, using rakes to collect the fruits and placing them in bags to be carried by wheelbarrows [8-9]. However, implementation of loose fruit collection using the current method entails some negative effects. Firstly, the manual rake and bag method introduces a substantial amount of debris. Ahmad *et al*., [10], Darius & Fairulnizam, [4] and Yusoff *et al*., [8] reported debris of 60%, 30-40 % and 20-30% respectively. High percentage of debris will lower OER [11]. As a solution, Shuib & Khalid, [12] introduced a separating machine to clear debris from the manually collected fruits. The machine however, only solves for debris clearing but not the other shortcomings of manual collections. Hence, an oil palm loose fruit collector is designed using the cyclone separator mechanism to curb the disadvantages of manual collections.

The design of cyclone separators is generally simple with minimal maintenance and variable working temperature, which is a main reason it is opted by the industry as a method for material separation. According to Park and Go [13], the working principle of the air cyclone separator is as materials are being sucked in through the inlet, a centrifugal force will act on the materials which forces them to the separator walls while the drag force acting on the materials forces them to the centre of the cyclone separator. Thus, heavy or course materials will remain on the walls, swirling down to be collected via the outer vortex of the cyclone separator while lighter fine materials that has been dragged to the centre of the cyclone where the inner vortex is located will be transported out of the system.

There are various parts of the cyclone separator regarded as critical to its performance. One of the most extensively studied parts is the vortex finder. A study conducted by Fu et al. [14], where they worked on evaluating the performance of slotted vortex finders. The vortex finders were slotted in order to deter swirling in the cortex finder and act as an inertial separator. This in turn will inhibit the escape of particles, resulting in more collection. The study observed an increase of collection efficiency of over 5 %. In addition, the design of the slotted vortex finder also resulted in pressure drops of up to 27.9%, where it discourages materials to enter the inner vortex and reduces the pressure drop. Wasilewski et al. [15] investigated the effects of varying vortex finder's length and diameter in square cyclone separators. They found that increasing the diameter of vortex finder lowered the pressure drop in the cyclone separator while length of vortex finder only caused slight differences in the pressure drop. Thus, it can be inferred that the diameter of a vortex finder has a more significant effect to cyclone mechanism if compared to length variations. Wei et al. [16] conducted a numerical study by varying the inlet and vortex finder dimensions, then used response surface methodology to determine the more significant factor. The results indicated the vortex finder diameter is more significant to the flow in a cyclone separator more than inlet variations. This finding has also imposed the importance of vortex finder to a cyclone operation. A study by Elsayed and Lacor [17], also supported the significance of vortex finder diameter as opposed to length where they found decreasing the vortex finder diameter by 40% resulted in 175% increase in pressure drop while increasing the length of vortex finder by 50% only increases pressure drop by 25%.

A previous study by Elsayed and Lacor [18], studied the effects of vortex finder diameter variations on the performance of a cyclone separator and found that a narrower vortex finder decreases cut off size of material separation. Yohana et al. [19] in another study found that decreasing vortex finder's diameter boost the separation efficiency. In another unique study, Kumar and Jha [20] proved considerable effect of optimizing the divergence and convergence of a vortex finder to the performance of a cyclone separator. The optimized design of the study showed good results in terms of having pressure drop without sacrificing separation efficiency as opposed from the study by El-Batsh [21], where increasing the vortex finder diameter lead to increase in pressure drop and deterioration in separation efficiency. The available literature explained the importance of vortex finder to pressure drop and its relationship to collection efficiencies in cyclone separators.

Hence, vortex finder of a cyclone separator serves as an important parameter in design considerations. In this study, the inlet air speed is being studied to assess its effects on the collection efficiency of the designed machine. Hence, computational fluid dynamics (CFD) is employed to further analyze the flow in the system. RSM and DPM is opted to numerically simulate the flow and material collection of the cyclone separator. The goal of the study is to evaluate the effects of vortex finder variations on the machines collection efficiency and pressure drop.

2. MATERIAL AND METHODS

2.1. Governing equations of the RSM

According to Ansys Fluent Theory Guide [22], RSM navigates the Reynolds-averaged Navier-Stokes (RANS) equations by solving the Reynolds stresses' transport equations alongside a dissipation rate equation. The model approaches effects of streamline curvature, swirl, rotation and also rapid variations in strain rates thoroughly, making the model essential in simulating cyclone flows.

The Reynolds stresses' transport equation is given as such:

$$\frac{\partial}{\partial t}(\rho_f \overline{u'_\iota u'_J}) + C_{ij} = D_{T,ij} + D_{L,ij} + P_{ij} + G_{ij} + \phi_{ij} + \varepsilon_{ij} + F_{ij} + S_u \quad (1)$$

where $\frac{\partial}{\partial t}(\rho_f \overline{u'_\iota u'_J})$ is the unsolved part of the RANS equation in tensor form, while C_{ij} , $D_{T,ij}$, $D_{L,ij}$, P_{ij} , G_{ij} , ϕ_{ij} , ε_{ij} , F_{ij} , S_u are the terms for equations of convection, turbulent diffusion, molecular diffusion, stress production, buoyancy production, pressure strain, dissipation, system rotation production and user defined source respectively.

In short, RSM functions to model and compute the unsolved equation, $\frac{\partial}{\partial t}(\rho_f \overline{u'_\iota u'_J})$ as shown in Equation (1) by solving the transport and dissipation equations. In producing the RANS equation, Reynolds Averaging is applied on the Navier-Stokes equation, resulting in:

$$\frac{\partial \rho}{\partial t} + \frac{\partial}{\partial x_i}(\rho u_i) = 0 \quad (2)$$

and

$$\frac{\partial}{\partial t}(\rho u_i) + \frac{\partial}{\partial x_j}(\rho u_i u_j) = \frac{\partial \rho}{\partial x_i} + \frac{\partial}{\partial x_j}\left[\mu\left(\frac{\partial u_l}{\partial x_j} + \frac{\partial u_j}{\partial x_i} - \frac{2}{3}\delta_{ij}\frac{\partial u_l}{\partial xl}\right)\right] \quad (3)$$

$$+\frac{\partial}{\partial t}(\rho_f \overline{u'_\iota u'_J}) \quad (4)$$

where equations (2) and (3) are the RANS equations while equation (4) is the resulting effects of turbulence to be solved by RSM.

Turbulent Diffusion, $D_{T,ij}$

Going deeper on how RSM solves equation (1) through its model, $D_{T,ij}$ is modelled by Ansys Fluent using an equation of scalar turbulent diffusivity. The equation is given as:

$$D_{T,ij} = \frac{\partial}{\partial x_k}\left(\frac{\mu_t}{\sigma_k}\frac{\partial \overline{u'_\iota u'_J}}{\partial x_k}\right) \quad (5)$$

where σ_k = 0.82 and the turbulent viscosity, μ_t is calculated using the exact formula used in the k-ε model:

$$\mu_t = \rho C_\mu \frac{k^2}{\varepsilon} \tag{6}$$

where $C_\mu = 0.09$, note that this constant used in RSM does not equal to the value used for k-ε models.

Pressure-Strain, ϕ_{ij}

In Ansys Fluent, the pressure-strain term is calculated and modelled automatically by the governing equation:

$$\phi_{ij} = \phi_{ij,1} + \phi_{ij,2} + \phi_{ij,w} \tag{7}$$

where $\phi_{ij,1}$, $\phi_{ij,2}$ and $\phi_{ij,w}$ are the slow pressure-strain term, rapid pressure-strain term and wall reflection term respectively.

RSM approaches the slow pressure-strain term, $\phi_{ij,1}$ by default using the equation:

$$\phi_{ij,1} = -C_1 \rho \frac{\varepsilon}{k} \left(\overline{u'_\iota u'_J} - \frac{2}{3}\delta_{ij} k \right) \tag{8}$$

where C_1 is constant 1.8.

On the other hand, the rapid pressure-strain term, $\phi_{ij,2}$ is modelled by the equation:

$$\phi_{ij,2} = -C_2 \left[\left(P_{ij} + F_{ij} + \frac{5}{6} G_{ij} - C_{ij} \right) - \frac{2}{3}\delta_{ij} \left(P + \frac{5}{6} G - C \right) \right] \tag{9}$$

where C_2 is 0.6, C is $0.5C_{kk}$ while P_{ij}, F_{ij}, G_{ij} and C_{ij} is as explained in equation (1).

The final term of the pressure-strain term which is the wall reflection term, $\phi_{ij,w}$ is rather complex as it functions to redistribute the normal stresses near the wall. The term is modelled using the equation:

$$\phi_{ij,w} = C'_1 \frac{\varepsilon}{k} \left(\overline{u'_k u'_m}\, n_k n_m \delta_{ij} - \frac{3}{2}\overline{u'_\iota u'_k}\, n_j n_k - \frac{3}{2}\overline{u'_J u'_k}\, n_i n_k \right) \frac{C_l k^{\frac{3}{2}}}{\varepsilon d}$$
$$+ C'_2 \left(\phi_{km,2} n_k n_m \delta_{ij} - \frac{3}{2}\phi_{ik,2} n_j n_k - \frac{3}{2}\phi_{jk,2} n_i n_k \right) \frac{C_l k^{\frac{3}{2}}}{\varepsilon d} \tag{10}$$

where C'_1 is 0.5, C'_2 is 0.3, $C_l = C_\mu^{\frac{3}{4}}$ where C_μ is 0.9, k is the von Karman constant with the value of 0.4187 while n_k and d is the $x_k$component of the unit and distance normal to the wall respectively

Buoyancy Production, G_{ij}

The effects of buoyancy modelled in RSM turbulent model is governed by the equations:

$$G_{ij} = -\rho\beta \left(g_i \overline{u'_J \theta} + g_J \overline{u'_\iota \theta} \right) \tag{11}$$

$$\overline{U_\iota \theta} = \frac{\mu_t}{Pr_t} \left(\frac{\partial T}{\partial x_i} \right) \tag{12}$$

where the Prandt number, Pr_t =0.85, which is the turbulent number for energy and β stands for the coefficient of thermal expansion which is further elaborated by the equation:

$$\beta = -\frac{1}{\rho} \left(\frac{\partial \rho}{\partial T} \right)_p \tag{13}$$

Solving equation (13) for buoyancy production in ideal gases, the following equation is obtained and modelled for RSM:

$$G_{ij} = -\frac{\mu_t}{Pr_t} \left(g_i \frac{\partial \rho}{\partial x_j} + g_j \frac{\partial \rho}{\partial x_i} \right) \tag{14}$$

Dissipation, ε_{ij}

In RSM, the dissipation rate in a turbulent system is modelled using the equation:

$$\varepsilon_{ij} = \delta_{ij}(\rho\varepsilon + Y_M) \quad (15)$$

where Y_M is the additional dilatation dissipation and ε is the scalar dissipation rate. It can be solved using the following expression:

$$Y_M = 2\rho\varepsilon {M_t}^2 \quad (16)$$

where M_t is defined as the Mach number and can be calculated using the formula:

$$M_t = \sqrt{\frac{k}{a^2}} \quad (17)$$

where a is the speed of sound. The scalar dissipation rate, ε which is present in both equations (15) and (16) is solved using the same transport equation used in the k- ε model. The equation is as follows:

$$\frac{\partial}{\partial t}(\rho\varepsilon) + \frac{\partial}{\partial x_i}(\rho\varepsilon u_i) = \frac{\partial}{\partial x_j}\left[\left(\mu + \frac{\mu_t}{\sigma_\varepsilon}\right)\frac{\partial\varepsilon}{\partial x_j}\right] C_{\varepsilon 1}\frac{1}{2}[P_{ii} + C_{\varepsilon 3}G_{ii}]\frac{\varepsilon}{k} - C_{\varepsilon 2}\rho\frac{\varepsilon^2}{k} + S_\varepsilon \quad (18)$$

where σ_ε , $C_{\varepsilon 1}$ and $C_{\varepsilon 2}$ is 1.0, 1.44 and 1.92 respectively while $C_{\varepsilon 3}$ is computed as a function of local flow direction relative to gravitational vector. S_ε is denoted as user-defined source term.

2.2 Discrete Phase Model

In general,the discrete phase model and multiphase model are two methods in calculating particle laden flows in a fluid using CFD DPM was opted bbecause the second injected phase only constitutes a small percentage of volume; and if the case indicates otherwise, the multiphase model should be used. Hence, the interactions between the particles can be ignored and DPM is used to calculate the interactions of the said particles in the fluid flow. The governing equations of DPM follows the Euler-Langrage approach where the fluid phase is treated as a continuum in solving the Navier-Stokes equations. In DPM, the trajectory of a single particle is governed numerically by equating its inertia to the forces acting on it. The equation is given as the following:

$$\frac{d\overrightarrow{u_p}}{dt} = F_D(\underset{u}{\rightarrow} - \underset{u_p}{\rightarrow}) + \frac{\vec{g}(\rho_p - \rho)}{\rho_p} + \underset{F}{\rightarrow} \quad (19)$$

where $\underset{u}{\rightarrow}$ = fluid phase velocity, $\underset{u_p}{\rightarrow}$ = particle velocity, μ = molecular velocity of the fluid, ρ = density of fluid, ρ_p = density of particle, $\underset{F}{\rightarrow}$ = additional acceleration, force per unit particle mass and $F_D(\underset{u}{\rightarrow} - \underset{u_p}{\rightarrow})$ = drag force per unit particle mass which can be further elaborated by the equation:

$$F_D = \frac{18\mu\, C_D Re}{\rho_p {d_p}^2\, 24} \quad (20)$$

where d_p = particle diameter and Re, the Reynolds number can be represented by the formula:

$$Re = \frac{\rho d_p|\overrightarrow{u_p} - \vec{u}|}{\mu} \quad (21)$$

while C_D, the drag coefficient from equation (20) is given by the formula, for spherical drag:

$$C_D = a_1 + \frac{a_2}{Re} + \frac{a_3}{Re^2} \quad (22)$$

where a_1, a_2 and a_3 are constants given by Morsi & Alexander (1972).

2.3 Numerical Model Validation

The cyclone geometry of Hoekstra's work [23] was replicated to determine the extent of accuracy the numerical model offers in developing an oil palm loose fruit collector. Pressure drop validation was performed by simulating the numerical model at velocities of 5, 7, 9, 10, 15, 18 and 20 ms^{-1}. This step ensures the solver settings in the numerical study behaves accurately and demonstrates reliable precision. Figure 1 shows a comparison of the numerical simulation to experimental work where the pressure drops were measured across varied inlet velocity using pressure differential sensors. As can be seen, the simulated data is in good agreement with experimental data where maximum percentage difference compared to experimental data were recorded at 7.5%.

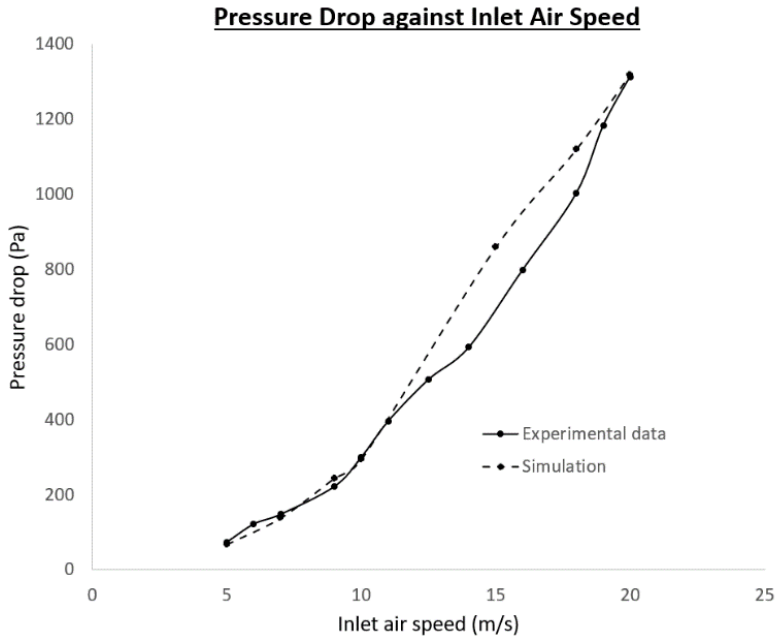

Figure 1. Pressure drop comparison between numerical simulation and experimental data.

Tangential velocity is an imperative indication of a cyclone separator performance. In Figure 2, it can be seen that the experimental data [23] and the simulated data from the present study exhibited the same pattern with minor deviations. The maximum error recorded was 14.98% in the profile at radial position of 0.58. However, for other regions the errors were very minimal and this showed that the numerical simulation obeys the cyclone separator mechanism as validated by experimental data. Verily, precisely close comparisons of the numerical study data with the works of Hoekstra are indications that the present work is consistent and of reasonable precision.

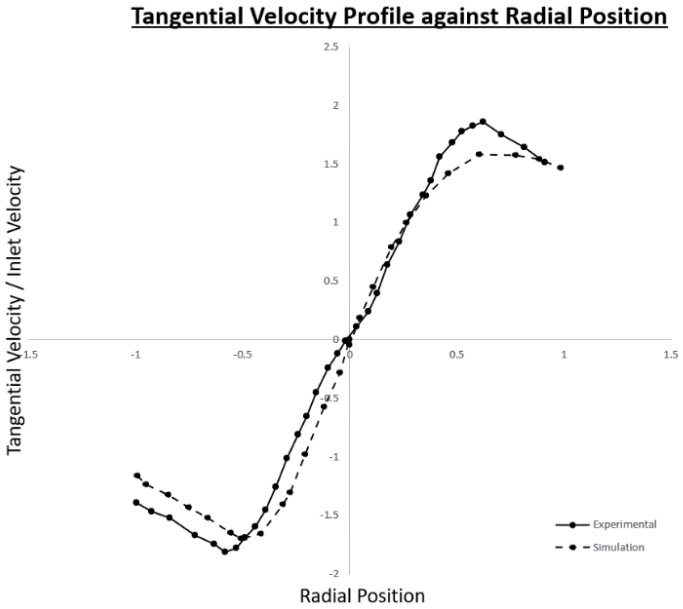

Figure 2. Tangential velocity comparison between numerical simulation and experimental data.

2.4 Cyclone geometry

The type of cyclone separator is an important design consideration as the swirl in the cyclone will affect their collection performance due to the difference in flow characteristics. In this study, several types of cyclone separator have been considered; 1D2D, 2D2D, and 1D3D cyclone separators. El-Emam *et al*., [24] investigated the performance of various cyclone separators and discovered that the 1D2D cyclone is the most effective among conventional cyclones. The first 'D' indicates the cyclone critical diameter, D_c while the second 'D' refers to the cyclone height in reference to D_c. A 1D2D cyclone separator will have a cyclone height double than that of D_c. Figure 1 provides a standard cyclone with its denoted parts.

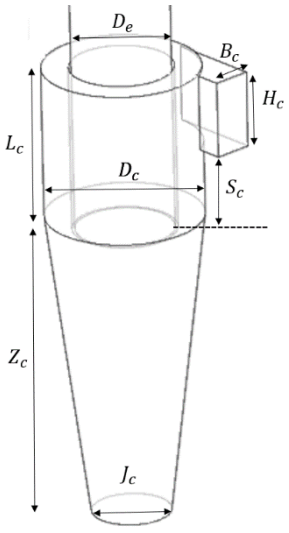

Figure 3. Standard cyclone separator.

2.5 Boundary Condition

Table 1 CFD solver settings used in the study.

Setting	Input
Gravity	9.81 m s^{-2}
Solver	Pressure based
Velocity formulation	Absolute
Time	Steady
Pressure-velocity coupling	SIMPLE
Spatial discretization (Pressure)	Second order
Spatial discretization (Momentum)	Second order upwind
Spatial discretization (Turbulent Kinetic Energy)	Second order upwind
Spatial discretization (Turbulent dissipation Energy)	Second order upwind
Spatial discretization (Energy)	Second order upwind

Table 2 Simulation runs in the study.

Simulation	Outlet diameter (m)	Vortex finder length (m)
1	0.12	0.27
2	0.12	0.405
3	0.18	0.405
4	0.18	0.27

Inlet velocity of 20 m/s was used in all of the simulation for data comparison purposes and DPM was used to simulate the cyclone flow field and loose fruit collection. Wall was set to a no slip condition with standard wall functions. Hydraulic diameter of the gas outlet is B_c=0.1 m. Hydraulic diameters of the particle's outlet are J_c=0.15 m and 0.2 m respectively. Turbulence intensity at the gas and particles outlet are specified at 5%. For the DPM an injection with density 995.7 kg/m^3 and 0.04 m was set to simulate oil palm loose fruit collection into the system [25]. Table 1 shows the solver settings used in the CFD. The outlet diameter and vortex finder length were studied at 2 levels resulting in 4 simulations as shown in Table 2. Effects of the variations were then evaluated based on the collection efficiency and pressure drop recorded.

Table 3 Dimensions of designed cyclone

Dimensions	First cyclone separator (mm)	Second cyclone separator (mm)
D_c	300	400
B_c	75	100
D_e	187.5	250
H_c	150	200
J_c	150	200
S_c	187.5	250
L_c	300	400
Z_c	600	800

Figure 4 depicts the labelled diagram of a two-stage cyclone separator used in the study with its dimensions listed in Table 3. Debris will be introduced into the smaller first stage cyclone separator as the loose fruits are collected via air suction through the inlet. Heavy loose fruits will be gathered via the outlet in the first stage cyclone separator, while lighter debris will be pulled through the vortex finder and collected in the second stage cyclone separator. Clean loose fruits will thus be collected by the first stage cyclone, while undesirable debris would be deposited in the second cyclone.

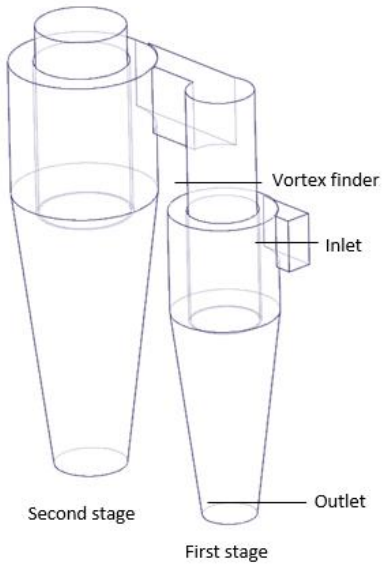

Figure 4. Cyclone separator design used in study

3. RESULTS AND DISCUSSIONS

3.1 Flow Analysis

In general, the flow inside the cyclone separator was satisfactory. Figures 5 and 6 shows the velocity and pressure vectors of the dual cyclone separators. From Figure 5, it can be seen that as air flows into the first cyclone, a high velocity is recorded and it increases to a maximum (red) near the walls where the velocity vectors proceeded to swirl into a vortex with decreasing velocity as the air travels further down. Then, at the bottom of the vortex in the first cyclone, it can be observed that an inner vortex is present where the directions of the velocity vector swirl up to the vortex finder into the second cyclone separator. A same pattern is observed in the second cyclone where the vectors indicate the presence of inner and outer vortexes. The theory of cyclone separator mechanism is confirmed in both dual cyclone separators by studying the velocity vectors. Referring to Figure 6, generally the pressure vectors showed similar patterns in both cyclone separators to velocity vectors.

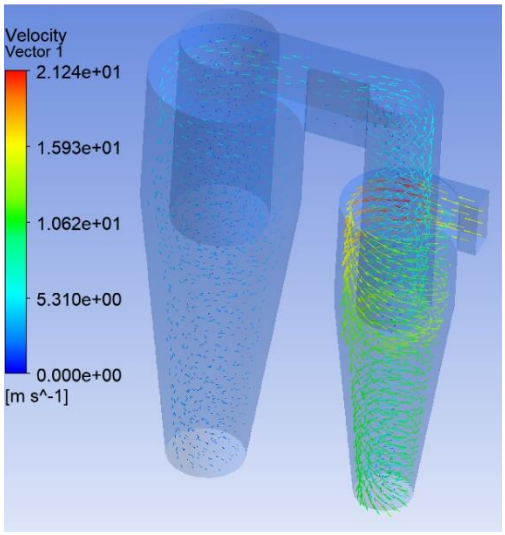

Figure 5. Velocity vectors in dual cyclone separators.

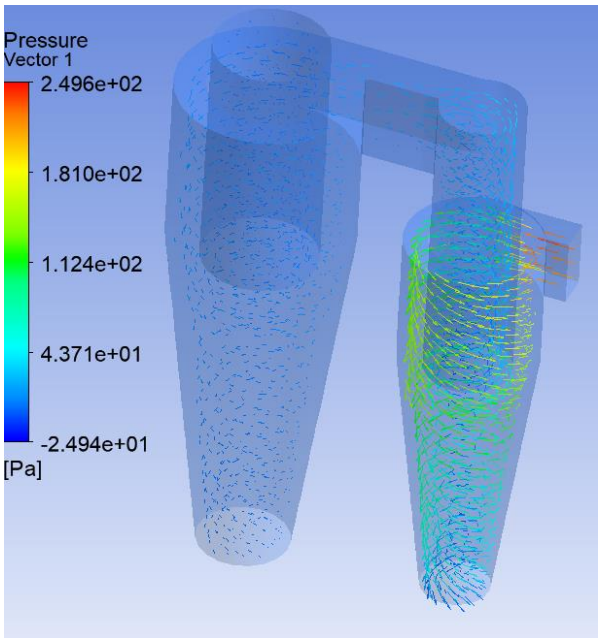

Figure 6. Pressure vectors in dual cyclone separators.

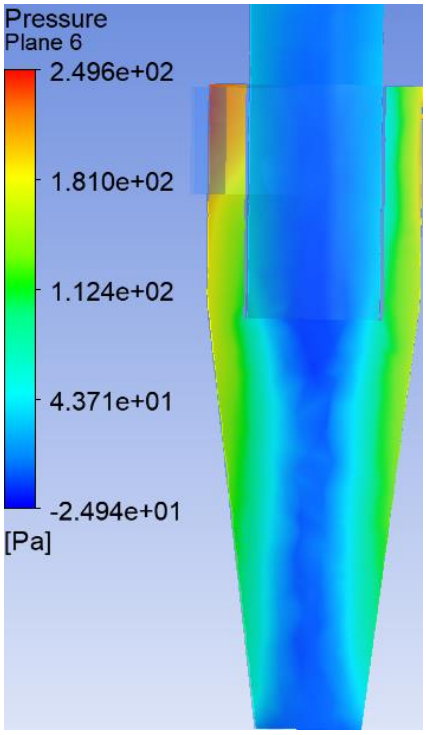

Figure 7. First cyclone pressure profile.

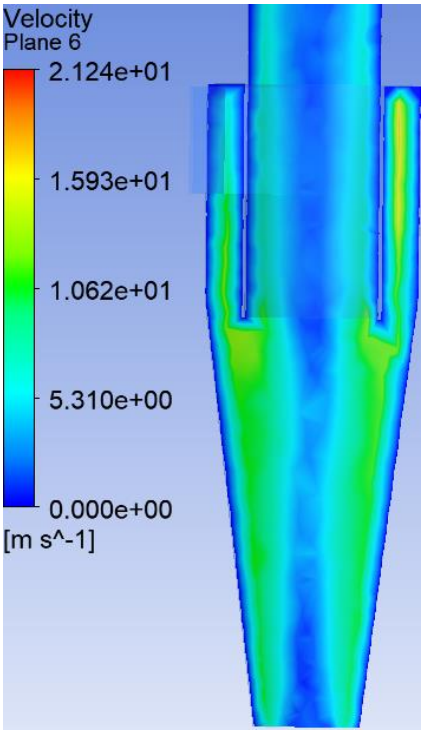

Figure 8. First cyclone velocity profile.

As can be seen from Figures 7 and 8, the profile for both pressure and velocity are both satisfactory, in accordance to the cyclone separator theory. The velocity at the walls is stagnant where blue shades are observed. In addition, the centre of the cyclone separator also observed stagnation flow, while the air swirls down the cyclone separator along the wall, the centre will experience a stagnation in speed while the inner vortex will transport lighter material out of the first cyclone. A Rankine vortex which explains the operation of a cyclone is confirmed [25].

3.2 Vortex finder length and outlet diameter effects

Table 4 Results from numerical simulations.

Exit diameter (m)	Vortex finder length (m)	Pressure drop (Pa)	Collection efficiency (%)
0.12	0.27	525.36	55.86
0.12	0.405	513.02	76.95
0.18	0.405	477.66	88.71
0.18	0.27	471.65	66.41

The main goal of varying the vortex finder geometry in term of its length and diameter is to achieve the most efficient machine in collecting oil palm loose fruits. Table 4 shows the results obtained in the numerical simulations conducted in the study. It is obvious that the highest collection efficiency recorded was at 88.71 % with an exit diameter of 0.18m and vortex finder length of 0.405m. Note that these are the maximum values applicable in the geometry of the machine due to the fact that increasing the dimensions above the specified levels will result in the inability of loose fruits passing through the collection system leading to clogging. On the other hand, the lowest collection efficiency recorded was 55.86 % with the minimums being employed as the factors. Thus, it is proven in the study a large vortex finder diameter and length is favourable for machine operation.

In terms of pressure drop, it was found that the vortex finder variations had little effect on the factor. The difference between measured pressure drops stands at a range between 2% to 10 % compared to the highest pressure drop recorded. This is due to the fact that the pressure drop relies heavily on the inlet collection speed which is identical in all the simulations at 20 m/s. Since all of the numerical simulations used the same inlet speed, little variations on the pressure drop were expected and proven.

4. CONCLUSION

Conclusively, a larger exit diameter with an increased vortex finder length is preferred for a more efficient oil palm loose fruit collector. However, besides vortex finder length and exit diameter variations, there are numerous parameters to consider such as the inlet air speed and cone variations. Thus, a more comprehensive study is needed to assess each parameter and their interactions with one another for an efficient and reliable oil palm loose fruit collector machine.

REFERENCES

[1] Malaysia Palm Oil Board (2020). Oil palm statistics. Area (2020). Retrieved from http://bepi.mpob.gov.my/index.php/en/?option=com_content&view=category&id=115

[2] Yusoff, M. Z. M., Zamri, Abd Kadir, M. Z. A., Wan Hassan, W. Z. & Azis, N. (2019). Loose collector machine in malaysia: a review. *International Journal of Engineering Technology and Sciences*. Vol. 6 (2).

[3] Khalid, M. R. & Shuib, A. R. (2017). Performance of oil palm loose fruits separating machine. Journal of Oil Palm Research. Vol. 29 (3). pp. 358-365. https://doi.org/10.21894/jopr.2017.2903.08

[4] Darius, E. P. & Fairulnizam, M. H. (2015) Effects of collecting systems and plantation environment on debris accumulation in a collected oil palm loose fruits. *Proc. Int. Conf. Plt. Phy. 2014*. pp. 147-151.

[5] Sime Darby (2008). Loose Fruit vs. Lost Income. Seedlink: A bimonthly publication by Sime Darby Sdn. Bhd., March 2008, Vol. 2/6. Subang Jaya. pp.8.

[6] Shuib, A. R., Khalid, M. R. & Bakri, M. A. M. (2018). Development of oil palm loose fruit collecting machine with elevated discharge mechanism. *International Journal of Engineering Research & Technology.* Vol. 7. Issue 10. pp. 225-234.

[7] Chang, L. C., Sani, A. R. A. & Basran, Z. An economic perspective of oil extraction rate in the oil palm industry of Malaysia. *Oil Palm Industry Economic Journal.* Vol. 3 (1). pp. 25-31.

[8] Yusoff, M. M. Z., A. Zamri, Abd Kadir, M. Z. A., Wan Hassan, W. Z. & Azis, N. (2020). Development of integrated loose fruit collector machine for oil palm plantation. *Bulletin of Electrical Engineering and Informatics*. Vol. 9. pp. 500-506.

[9] Sukadarin, E. H., Deros, B. M., Nawi N. S. M., Ghani, J. A., Ismail, A. R. & Zakaria, J. (2016). Back pain and the observed factor among oil palm workers, *International Journal of International Technology and Sciences*. Vol. 5. pp. 70-78.

[10] Ahmad, H., Ahmad Zamri, M.Y, & Mohd S. J. (1995). Loose Fruit Collector. PORIM Information Series No.19, Palm Oil Research Institute of Malaysia (PORIM), Selangor.

[11] Khalid, M. R. & Shuib, A. R. (2017). Performance of oil palm loose fruits separating machine. *Journal of Oil Palm Research.* Vol. 29 (3). pp. 358-365.

[12] Shuib, A. R. & Khalid, M.R. (2005). Air-Assisted Loose Fruit Separating Machine, MPOB Information Series No.261, Malaysia Palm Oil Board (MPOB), Selangor.

[13] Park, D. & Go, J. (2020). Design of Cyclone Separator Critical Diameter Model Based on Machine Learning and CFD. Processes. 8. 10.3390/pr8111521.

[14] Fu, S., Zhou, F., Sun, G., Yuan, H. & Zhu, J. (2021). Performance evaluation of industrial large-scale cyclone separator with novel vortex finder. *Advanced Powder Technology.* 32. pp. 931–939.

[15] Wasilewski, M., Brar, L. & Ligus, G. (2020). Experimental and numerical investigation on the performance of square cyclones with different vortex finder configurations. *Separation and Purification Technology*. 239. 116588.

[16] Wei, Q., Sun, G. Gao, C. (2020). Numerical analysis of axial gas flow in cyclone separators with different vortex finder diameters and inlet dimensions*. Powder Technology*. Volume 369. pp. 321-333.

[17] Elsayed, K. & Lacor, C. (2010). The effect of vortex finder diameter on cyclone separator performance and flow field. *V European Conference on Computational Fluid Dynamics. 14-17 June 2010.*

[18] Elsayed, K. & Lacor, C. (2013). The effect of cyclone vortex finder dimensions on the flow pattern and performance using LES. *Computers & Fluids.* Volume 71. pp.224-239.

[19] Yohana, E., Tauviqirrahman, M., Putra, A. R., Ade, E. D. & Choi, K. H. (2018). Numerical analysis on the effect of the vortex finder diameter and the length of vortex limiter on the flow field and particle collection in a new cyclone separator. *Cogent Engineering*. 5:1. 1562319

[20] Kumar, V. Jha, K. (2019). Multi-objective shape optimization of vortex finders in cyclone separators using response surface methodology and genetic algorithms. *Separation and Purification Technology*. Volume 215, pp. 25-31.

[21] El-Batsh. H. M. (2013). Improving cyclone performance by proper selection of the exit pipe. *Applied Mathematical Modelling.* Volume 37. Issue 7. pp. 5286-5303.

[22] ANSYS FLUENT Theory Guide, ANSYS, Inc., Release 15.0, November 2013.

[23] Hoekstra, AJ., Derksen, JJ., & Van Den Akker, HEA. (1999). An experimental and numerical study of turbulent swirling flow in gas cyclones. Chemical Engineering Science, 54(13-14), pp. 2055-2065.

[24] El-Emam, M. A., Zhou, L., Shi, W. & Han, C. (2021). Performance evaluation of standard cyclone separators by using CFD–DEM simulation with realistic bio-particulate matter. *Powder Technology*. Volume 385. pp. 357-374. https://doi.org/10.1016/j.powtec.2021.03.006